A method for the direct measurement of electronic site populations in a molecular aggregate using two-dimensional electronic-vibrational spectroscopy

Nicholas H. C. Lewis, Hui Dong, Thomas A. A. Oliver, and Graham R. Fleming

Citation: The Journal of Chemical Physics **143**, 124203 (2015); doi: 10.1063/1.4931634
View online: http://dx.doi.org/10.1063/1.4931634
View Table of Contents: http://scitation.aip.org/content/aip/journal/jcp/143/12?ver=pdfcov
Published by the AIP Publishing

A method for the direct measurement of electronic site populations in a molecular aggregate using two-dimensional electronic-vibrational spectroscopy

Nicholas H. C. Lewis, Hui Dong, Thomas A. A. Oliver,[a] and Graham R. Fleming[b]
Department of Chemistry, University of California, Berkeley, California 94720, USA;
Physical Biosciences Division, Lawrence Berkeley National Laboratory, Berkeley, California 94720, USA;
and Kavli Energy Nanosciences Institute at Berkeley, Berkeley, California 94720, USA

(Received 8 July 2015; accepted 9 September 2015; published online 28 September 2015)

Two dimensional electronic spectroscopy has proved to be a valuable experimental technique to reveal electronic excitation dynamics in photosynthetic pigment-protein complexes, nanoscale semiconductors, organic photovoltaic materials, and many other types of systems. It does not, however, provide direct information concerning the spatial structure and dynamics of excitons. 2D infrared spectroscopy has become a widely used tool for studying structural dynamics but is incapable of directly providing information concerning electronic excited states. 2D electronic-vibrational (2DEV) spectroscopy provides a link between these domains, directly connecting the electronic excitation with the vibrational structure of the system under study. In this work, we derive response functions for the 2DEV spectrum of a molecular dimer and propose a method by which 2DEV spectra could be used to directly measure the electronic site populations as a function of time following the initial electronic excitation. We present results from the response function simulations which show that our proposed approach is substantially valid. This method provides, to our knowledge, the first direct experimental method for measuring the electronic excited state dynamics in the spatial domain, on the molecular scale. © *2015 AIP Publishing LLC.* [http://dx.doi.org/10.1063/1.4931634]

I. INTRODUCTION

Photosynthetic pigment-protein complexes perform a number of distinct tasks, including light harvesting, exciton migration, dissipation of excess energy, and the separation and transfer of charge carriers.[1–3] They are able to perform these tasks with only a relatively small molecular toolbox, consisting primarily of a variety of chlorin derivatives and carotenoids. Photosynthetic organisms are able to use this small toolbox to significant advantage, tuning the properties towards specific roles. They accomplish this by precisely controlling the spatial organization and the local environments of the pigments to tune the electronic structure of the complex, affecting the electronic energies of each pigment as well as the strength of the coupling between neighboring molecules. These interactions result in varying degrees of delocalization in the electronic excited states and help to guide both the energetic and the spatial dynamics of the electronic excitation energy.

In recent years, two-dimensional electronic spectroscopy (2DES) has become a mature technique for studying electronic dynamics in photosynthetic complexes, as well as other types of molecular aggregates.[4,5] Much progress towards the understanding of electronic excitation dynamics in these types of systems has been enabled by this technique, with the determination of precise energetic pathways and unraveling of the degree to which electronic coherence may, or may not, determine the rate and efficiency of energy transfer.[6–14] All of these applications of electronic spectroscopies, however, critically rely on the development of accurate models to provide the link between the electronic energy levels and the spatial character of the states. Typically, these models rely on incomplete information regarding both the electronic and spatial structures of these complexes and necessitate complicated procedures that aim to optimize the fit to a number of different, but related, observables, such as the spectral structures in 2DES and various linear spectra.[15–18] It has been demonstrated that the polarization dependence of 2DES can provide structural information that helps constrain the parameters of the model,[19,20] but this crucially relies on complex mutant studies to link the excitons with their spatial locations. Imperfections in the model still have substantial ramifications for the results, potentially resulting in an incorrect interpretation of the spatial localization of the excitation due to the difficulty in correctly separating the site energies from the strength of the electronic coupling. The information derived from this model-based approach has been very successfully applied towards the accurate reproduction of experimental observables in even very large and complex systems,[21] and recent developments in highly scalable electronic structure methods show promise in aiding the future refinement of these models.[22] To improve feedback between theory and experiment, however, there is a distinct need for an experimental method capable of directly linking the energetic and spatial domains without need for a model, or the assumptions that this entails.

Electronic spectroscopies, like 2DES, are very useful for understanding energetic structure and dynamics in complicated

[a]Current address: School of Chemistry, University of Bristol, Bristol BS8 1TS, United Kingdom.
[b]Electronic mail: grfleming@lbl.gov

systems, but they lack a direct connection to spatial information. Alternatively, vibrational spectroscopies are capable of providing structural information, and 2D infrared spectroscopy (2DIR) has become a widespread tool in the study of protein structure and structural dynamics.[23,24] Pure vibrational spectroscopy does not, however, provide any information about electronic dynamics. The recently developed 2D electronic-vibrational (2DEV) spectroscopy provides a direct link between these two regimes.[25] 2DEV measures the direct correlation between electronic and vibrational degrees of freedom, providing the cross peak between the traditional 2DES and 2DIR spectra. The successful application of 2DEV to the study of molecular aggregates, such as photosynthetic pigment protein complexes, has the potential to provide a direct experimental connection between the energetic and spatial domains of electronic energy transfer that has heretofore been missing.

We propose a method by which 2DEV spectra of a molecular aggregate could be used to directly measure electronic site populations, without need for a model. This method is based on the idea that a localized vibrational mode that is only weakly coupled to the electronic transition of interest could be used as a proxy for spatial location in an extended molecule or aggregate. This idea of using localized vibrations as proxies for position in a molecular aggregate has been used previously in the analysis of visible-infrared pump-probe spectroscopy[26,27] and is similar to the idea of using high frequency vibrational modes to monitor conformational dynamics commonly found in the analysis of femtosecond stimulated Raman spectroscopy.[28,29] The extension of the method to a multidimensional technique, in which both the excitation axis and the detection axis are resolved, allows for much greater detail in the information extracted from the spectra. Indeed, the approach described here not only provides the rates of energy transfer and relaxation, but also, without approximation, enables the extraction of electronic populations in the site basis.

The specific method that we propose in this work is not without its flaws and, indeed, is not entirely general. It crucially relies on the ability to resolve a spectral feature corresponding to each electronic excited state and a vibration localized on each monomer. In our spectral simulations, the parameters have been chosen to provide an illustrative example. Our goal here is not to provide a fully general analysis method that will work with spectra where these conditions are not met, but rather to demonstrate that in principle, the information can be extracted with a relatively straightforward technique. To this end, it important to note the distinction between the approximate model we use to provide illustrative simulations and the method used to extract the information from these approximate spectra, which is not subject to the same approximations.

In this work, we extend the response functions recently developed for simulating the 2DEV spectra of a monomer, and successfully applied to the study of correlated electronic and vibrational spectral dynamics and disorder,[30,31] to the case of a molecular dimer. We then describe how these spectra can be used to directly measure the electronic site populations in a generic molecular aggregate without need for an accompanying model. Finally, we use the response function simulations to provide a numerical demonstration of this method for the dimer case, which shows that the resulting measured populations are exactly equal to those from a direct calculation using a quantum master equation with the same dynamical model.

II. MODEL

A. Dimer Hamiltonian

To demonstrate the feasibility of the proposed measurement, we use a simplified model to describe the system. A schematic illustration of this model is shown in Figure 1. The Hamiltonian for our model is given by

$$H = H^A + H^B + J\left(|e_A\rangle\langle e_B| + |e_B\rangle\langle e_A|\right), \tag{1}$$

where H^A and H^B are the Hamiltonians for the monomers A and B, J is the electronic coupling, and $|e_A\rangle$ and $|e_B\rangle$ are the electronic excited states for the monomers. The monomer Hamiltonians are taken to be the same as in our previous studies of the 2DEV spectra of a solvated dye molecule[30,31] and are considered as four-level systems with the form

$$\begin{aligned} H^M = {} & H^M_{bath} + H^M_{g1}|g_M 1\rangle\langle g_M 1| \\ & + H^M_{e0}|e_M 0\rangle\langle e_M 0| + H^M_{e1}|e_M 1\rangle\langle e_M 1|, \end{aligned} \tag{2}$$

where each of the terms is defined as

$$H^M_{bath} = \hbar\sum_i \omega_i^M a_i^{M\dagger} a_i^M + \hbar\sum_j \nu_j^M b_j^{M\dagger} b_j^M, \tag{3}$$

$$H^M_{g1} = \hbar\omega_M + \hbar\sum_j h_j^M \nu_j^M \left(b_j^{M\dagger} + b_j^M\right), \tag{4}$$

$$\begin{aligned} H^M_{e0} = {} & \epsilon_M + \hbar\sum_i d_i^M \omega_i^M \left(a_i^{M\dagger} + a_i^M\right) \\ & + \hbar\sum_j \alpha_0^M h_j^M \nu_j^M \left(b_j^{M\dagger} + b_j^M\right), \end{aligned} \tag{5}$$

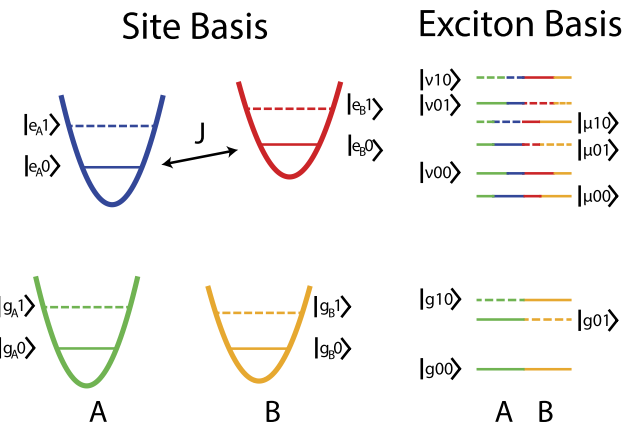

FIG. 1. A schematic illustration of the model used in this work (energies are not drawn to scale). The electronic ground state is indicated by green for monomer A and yellow for monomer B, whereas the electronic excited state is indicated by blue and red, respectively. Solid lines indicate that the vibration is on the ground state, while dashed lines indicate that the vibration is excited. Note that when one of the excitons is populated, a vibrational excitation can occur with that monomer on either the ground or excited electronic state.

$$H_{e1}^{M} = \epsilon_M + \hbar\omega'_M + \hbar\sum_i d_i^M \omega_i^M \left(a_i^{M\dagger} + a_i^M\right) + \hbar\sum_j \alpha_1^M h_j^M \nu_j^M \left(b_j^{M\dagger} + b_j^M\right). \quad (6)$$

Here, $M = A$ or B labels the monomers. We define ϵ_M as the electronic energy gap, while ω_M and ω'_M are defined as the frequency of the probed vibrational mode when monomer M is on the ground (ω_M) or excited (ω'_M) electronic state. H_{bath}^M denotes the Hamiltonian for the environment, and the operators a_i^M $\left(a_i^{M\dagger}\right)$ and b_j^M $\left(b_j^{M\dagger}\right)$ are the annihilation (creation) operators for the bath degrees of freedom for the electronic and vibrational modes, respectively, which are taken to be harmonic oscillators with frequencies ω_i^M and ν_j^M. The electronic and vibrational degrees of freedom on each monomer are all assumed to have completely independent baths. The parameters d_i^M and h_j^M describe the strength of the system-bath coupling for the electronic and vibrational degrees of freedom. These system-bath coupling components of the Hamiltonian are typically characterized by spectral densities, defined as $\mathcal{J}_e^M(\omega) = \sum_i {d_i^M}^2 {\omega_i^M}^2 \delta(\omega - \omega_i^M)$ and $\mathcal{J}_v^M(\omega) = \sum_j {h_j^M}^2 {\nu_j^M}^2 \delta(\omega - \nu_j^M)$ for the electronic and vibrational levels, respectively. The coupling between the electronic and vibrational system degrees of freedom is included via the change in the frequency of the vibration and the parameters α_0^M and α_1^M, which rescale the strength of the vibration-bath coupling due to the electronic excitation.[30,31] We have shown previously how these parameters can be extracted from the 2DEV spectra of a monomer.[31]

In choosing this form for the monomer Hamiltonians, we have made several assumptions and approximations. First of all, we assume that the laser used to drive the electronic transition only excites the fundamental 0-0 transition in the vibration that is being probed and does not excite higher vibronic transitions, either due to insufficient bandwidth or small Franck-Condon factors. This assumption allows us to consider the monomers as four-level systems and greatly reduces the number of pathways that must be considered, simplifying the resulting spectra. It also allows us to neglect any displacement in the equilibrium position of the vibration that is probed, the dominant effect of which would be to modify the Franck-Condon factors and shift the oscillator strength of the electronic transition towards higher vibronic transitions. Additionally, we assume that the monomer Hamiltonian is diagonal in the basis $\{|g_M 0\rangle, |g_M 1\rangle, |e_M 0\rangle, |e_M 1\rangle\}$, and therefore, we neglect relaxation of the electronic and vibrationally excited states. In photosynthetic light harvesting complexes, electronic relaxation to the ground state typically occurs on a much longer time scale (~100 ps–1 ns) than the energy transfer processes (~100 fs–1 ps) we are concerned with here and should be easily separable from the desired information using our proposed procedure. Neglecting vibrational relaxation should not have a significant effect due to the assumption that the initial excitation only involves the ground vibrational states. Because of this assumption, the vibrational lifetime will primarily contribute via its effects on the vibrational linewidth, which will not have a significant impact on the quantities that are the focus of this work.

For the interaction between the monomers, we include an electronic coupling term, characterized by the parameter J. The electronic coupling serves to mix the electronic states and form delocalized excitons, labelled $|\mu\rangle$ and $|\nu\rangle$, with the form

$$\begin{aligned} |\mu\rangle &= \cos\theta\,|e_A\rangle + \sin\theta\,|e_B\rangle, \\ |\nu\rangle &= -\sin\theta\,|e_A\rangle + \cos\theta\,|e_B\rangle, \end{aligned} \quad (7)$$

where the mixing angle θ depends on the strength of the electronic coupling J and the difference in electronic site energies and is given by

$$\tan 2\theta = \frac{2J}{\bar{\epsilon}_A - \bar{\epsilon}_B}, \quad (8)$$

where $\bar{\epsilon}_M = \epsilon_M + \lambda_e^M + \alpha_0^{M^2}\lambda_v^M$ is the electronic transition energy on monomer M renormalized by the environmental reorganization energy for the electronic transition. The reorganization energy is related to the spectral density by $\lambda_x^M = \hbar\int_0^\infty d\omega\, \mathcal{J}_x^M(\omega)/\omega$, with $x = e$ or v. Using this analytic form for the diagonalization of the Hamiltonian, we have four total electronic states for the system, the ground state $|g\rangle$, the two exciton states $|\mu\rangle$ and $|\nu\rangle$, and the doubly excited state $|f\rangle$, which is not accessible in the current experiment and will not be considered further. The overall state of the system can then be described as $|\varepsilon\, v_A\, v_B\rangle$, where ε denotes the electronic state, and v_A and v_B denote the vibrational quantum number for monomers A and B, respectively. The exciton energies are $\epsilon_\mu = (\epsilon_A + \epsilon_B)/2 + \mathrm{sign}(J)\sqrt{(\epsilon_A - \epsilon_B)^2 + 4J}$, and $\epsilon_\nu = (\epsilon_A + \epsilon_B)/2 - \mathrm{sign}(J)\sqrt{(\epsilon_A - \epsilon_B)^2 + 4J}$. Throughout this work, we use capital roman letter to index sites, lowercase greek letters to index excitons, and lowercase roman letters to index other quantities. In particular, when we refer to the specific case of the dimer, we use μ and ν to denote the excitons, and A and B to denote the sites, whereas α, β, γ, and δ are used to denote generic excitons, and M and N are used to denote generic sites, in the case of the dimer as well as in the case of a larger molecular aggregate.

We assume that the coupling only induces mixing between the electronic states, and that the vibrations have no role in the mixing and remain localized on the monomers. This should be a reasonable approximation for the range of parameter values considered here, where the energies of the vibrations are substantially larger than the energy gaps between the electronic states. Furthermore, for the method we propose here, all that are required is that there exists a vibrational mode on each monomer that has these properties. This will likely always be the case, even when other modes are strongly mixed with the electronic states. The inclusion of vibronic mixing and the study of its effects on the structure of the 2DEV spectra would be very interesting, but the details become complicated, and a proper treatment would require a more sophisticated method for solving the quantum dynamics than used in this study.[32–36] We leave the incorporation of these effects for future work.

The total Hamiltonian can be rewritten in the exciton representation as

$$
\begin{aligned}
H = {} & H^A_{bath} + H^B_{bath} + H^A_{g1}|g1\rangle\langle g1| + H^B_{g1}|g01\rangle\langle g01| + \left(H^A_{e0}\cos^2\theta + H^B_{e0}\sin^2\theta + J\sin 2\theta\right)|\mu 00\rangle\langle\mu 00| \\
& + H^A_{e1}\cos^2\theta|\mu 10\rangle\langle\mu 10| + H^B_{e1}\sin^2\theta|\mu 01\rangle\langle\mu 01| + \left(H^A_{e0}\sin^2\theta + H^B_{e0}\cos^2\theta - J\sin 2\theta\right)|\nu 00\rangle\langle\nu 00| \\
& + H^A_{e1}\sin^2\theta|\nu 10\rangle\langle\nu 10| + H^B_{e1}\cos^2\theta|\nu 01\rangle\langle\nu 01| - \left[\left(H^A_{e0} - H^B_{e0}\right)\frac{\sin 2\theta}{2} - 2J\cos 2\theta\right]\left(|\mu 00\rangle\langle\nu 00| + |\nu 00\rangle\langle\mu 00|\right) \\
& - H^A_{e1}\frac{\sin 2\theta}{2}\left(|\mu 10\rangle\langle\nu 10| + |\nu 10\rangle\langle\mu 10|\right) + H^B_{e1}\frac{\sin 2\theta}{2}\left(|\mu 01\rangle\langle\nu 01| + |\nu 01\rangle\langle\mu 01|\right). \qquad (9)
\end{aligned}
$$

In the derivations of the response functions used in this work, it is necessary for us to neglect the terms of the Hamiltonian that go as $(|\mu\ldots\rangle\langle\nu\ldots| + |\nu\ldots\rangle\langle\mu\ldots|)$, which drive energy transfer between the excitons. To account for energy transfer processes, we include the dynamics in an *ad hoc* manner similar to that used previously in the development of response functions for energy transfer and reactive systems,[37,38] modified so that the dynamics are equivalent to Redfield theory under the secular approximation.[39,40] The details of the method by which we include these dynamics in the response functions are given in Appendix A.

To be precise, we use excited state dynamics that are fully determined by rates of population transfer. The rates are taken from Redfield theory, which is based on a second order perturbative expansion of the system-bath coupling terms in the Hamiltonian, together with a Markov approximation.[39,40] For a generic molecular aggregate, the Redfield relaxation tensor is given by

$$
\mathcal{R}_{\alpha\beta,\gamma\delta} = \Gamma_{\delta\beta,\alpha\gamma} + \Gamma^*_{\gamma\alpha,\beta\delta} - \delta_{\beta\delta}\sum_\kappa \Gamma_{\alpha\kappa,\kappa\gamma} - \delta_{\alpha\gamma}\sum_\kappa \Gamma^*_{\beta\kappa,\kappa\delta} \qquad (10)
$$

with the damping matrix

$$
\Gamma_{\alpha\beta,\gamma\delta} = \frac{1}{\hbar^2}\sum_{M,N}\langle\alpha|V_M|\beta\rangle\langle\gamma|V_N|\delta\rangle C_{MN}[\omega_{\delta\gamma}]. \qquad (11)
$$

Here, $V_M = \hbar\sum_i d^M_i\omega^M_i\left(a^{M\dagger}_i + a^M_i\right)$ is the system-bath coupling operator for the electronic degrees of freedom, $C_{MN}[\omega]$ is the Fourier-Laplace transform of the environment correlation function, and $\hbar\omega_{\alpha\beta} = \epsilon_\alpha - \epsilon_\beta$ is the difference energy between excitons α and β. The indices α, β, γ, and δ run over the electronic states, expressed in the exciton basis, and M and N run over the sites. With the Redfield tensor defined in this way, the dynamics of the density matrix are given by the Redfield master equation

$$
\frac{\partial}{\partial t}\rho_{\alpha\beta} = -i\omega_{\alpha\beta}\rho_{\alpha\beta}(t) + \sum_{\gamma,\delta}\mathcal{R}_{\alpha\beta,\gamma\delta}\rho_{\gamma\delta}(t). \qquad (12)
$$

The element $\mathcal{R}_{\alpha\beta,\gamma\delta}$ represents the rate of exchange from state $|\gamma\rangle\langle\delta|$ to state $|\alpha\rangle\langle\beta|$. In the full Redfield theory, any of these elements may take nonzero values. Therefore, any pair of elements in the density matrix, either population or coherence, might be coupled. By considering only the rates of population transfer, we are making the secular approximation, whereby when $|\omega_{\alpha\beta} - \omega_{\gamma\delta}| \neq 0$, we set $\mathcal{R}_{\alpha\beta,\gamma\delta} = 0$. This serves to decouple the dynamics of populations and coherences and significantly simplifies the interpretation of the dynamics and the derivation of the response functions. In general, it is not a good approximation,[41,42] but it provides a sufficient illustration for the purposes of this work. A demonstration that the dynamics used in the response functions in this work are equivalent to the secular Redfield theory is provided in Appendix B.

B. Response functions

The double-sided Feynman diagrams for the Liouville pathways included in the present approximate description are shown in Figure 2. In this section, we restrict our focus to the specific case of the dimer, though the results can be extended to a larger molecular aggregate.[16,43] Only the diagrams corresponding to rephasing pathways are depicted, and for each, there is a corresponding nonrephasing pathway, which differs by a complex conjugation of the state during t_1. Due to the very large difference in the frequencies of the electronic and vibrational coherences during the t_1 and t_3 periods, these pathways do not possess a significant rephasing power, and so, the information content of the rephasing and nonrephasing pathways is essentially equivalent.[30] Despite this, we maintain this language here to make a clear connection with degenerate spectroscopies. The response functions have the form

$$
\begin{aligned}
R^R_{\alpha M}(t_1,t_2,t_3) &= \left\langle|\vec{\mu}_\alpha|^2|\vec{\mu}_M|^2\right\rangle \\
&\quad\times\exp\left[i\frac{\overline{\epsilon}_\alpha}{\hbar}t_1 - i\overline{\omega}_M t_3\right]F^R_{\alpha M}(t_1,t_2,t_3), \\
R^{NR}_{\alpha M}(t_1,t_2,t_3) &= \left\langle|\vec{\mu}_\alpha|^2|\vec{\mu}_M|^2\right\rangle \\
&\quad\times\exp\left[-i\frac{\overline{\epsilon}_\alpha}{\hbar}t_1 - i\overline{\omega}_M t_3\right]F^{NR}_{\alpha M}(t_1,t_2,t_3),
\end{aligned} \qquad (13)
$$

for the rephasing and nonrephasing pathways on the ground electronic state. The angled brackets represent an orientational average, and the transition dipole moment $\vec{\mu}_\alpha$ corresponds to the transition between the ground state and exciton $|\alpha\rangle$, whereas the factor $\vec{\mu}_M$ corresponds to the transition dipole moment for the $0 \rightarrow 1$ transition for the vibration on site M, on the electronic ground state. The coherence factor oscillates during the time period t_1 at the renormalized exciton frequency $\overline{\epsilon}_\alpha/\hbar = (\epsilon_\alpha + \lambda_\alpha)/\hbar$ and at the renormalized vibrational frequency $\overline{\omega}_M = \omega_M + \lambda^M_v/\hbar$ during the time period t_3. The factors $F_{\alpha M}(t_1,t_2,t_3)$ are the third-order lineshape functions and can be written in terms of the linear lineshape functions which describe the bath induced fluctuations in the energies of the electronic and vibrational states, $g^A_e(t)$, $g^B_e(t)$, $g^A_v(t)$, and $g^B_v(t)$, which in turn can be directly calculated from the spectral densities for the different components of the bath.[43,44]

The pathways that evolve on the electronic excited state during t_2 have a similar structure, with a few important differences. They take the form

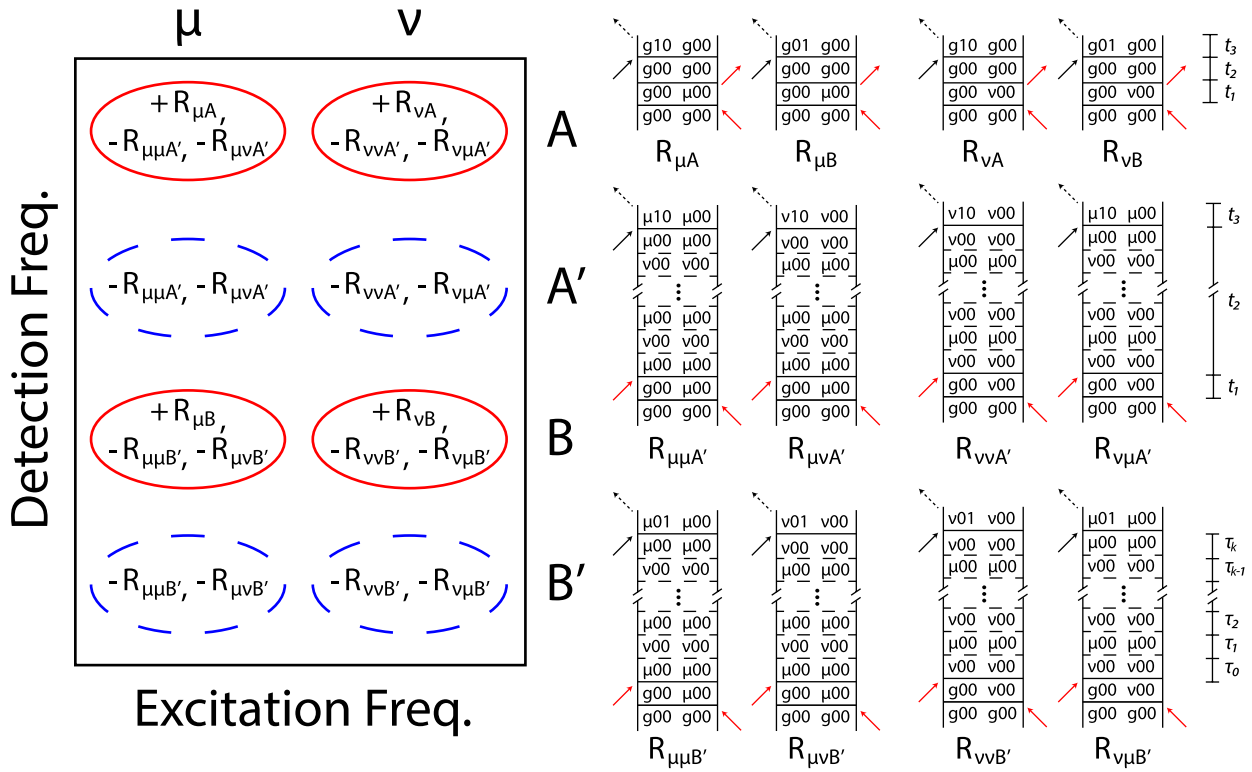

FIG. 2. The rephasing Liouville pathways considered in this work and a schematic illustration of the resulting spectrum. The pathways that evolve on the electronic ground state are labelled as $R_{\alpha M}$ to indicate that exciton $|\alpha\rangle$ is excited, and the vibration on site M is probed, while those on the electronic excited state are labelled as $R_{\alpha\beta M'}$ to indicate that the population is transferred from exciton $|\alpha\rangle$ to exciton $|\beta\rangle$ during t_2 and that the vibration on site M is probed. The interactions with the visible laser are indicated by red arrows while the interactions with the infrared laser are indicated by black arrows, and the emission of the infrared signals is indicated by the black dashed arrows. Within the current approximations, the pathways that evolve on the electronic ground state during t_2 have positive contributions (solid red lines), while the pathways that evolve on an electronic excited state make negative contributions (dashed blue lines). The plus and minus signs are present to emphasize the sign of each contribution to the total response. The time variables $\{\tau_i\}$ are used to describe the details of the trajectory on the electronic excited state.

$$R^{R}_{\alpha\beta M'}(t_1,t_2,t_3) = -\left(\left\langle|\vec{\mu}_\alpha|^2|\vec{\mu}_{M'}|^2\right\rangle|U_{\beta M}|^2\exp\left[i\frac{\overline{\epsilon}_\alpha}{\hbar}t_1 - i\overline{\omega}'_M t_3\right]\right.$$
$$\left. + \left\langle|\vec{\mu}_\alpha|^2|\vec{\mu}_M|^2\right\rangle\left(1-|U_{\beta M}|^2\right)\exp\left[i\frac{\overline{\epsilon}_\alpha}{\hbar}t_1 - i\overline{\omega}_M t_3\right]\right)F^{R}_{\alpha\beta M'}(t_1,t_2,t_3), \quad (14)$$

$$R^{NR}_{\alpha\beta M'}(t_1,t_2,t_3) = -\left(\left\langle|\vec{\mu}_\alpha|^2|\vec{\mu}_{M'}|^2\right\rangle|U_{\beta M}|^2\exp\left[-i\frac{\overline{\epsilon}_\alpha}{\hbar}t_1 - i\overline{\omega}'_M t_3\right]\right.$$
$$\left. + \left\langle|\vec{\mu}_\alpha|^2|\vec{\mu}_M|^2\right\rangle\left(1-|U_{\beta M}|^2\right)\exp\left[-i\frac{\overline{\epsilon}_\alpha}{\hbar}t_1 - i\overline{\omega}_M t_3\right]\right)F^{NR}_{\alpha\beta M'}(t_1,t_2,t_3), \quad (15)$$

where α is the initial excitonic state and β is the final excitonic state. Note that α and β may or may not be equal. The factor $\overline{\omega}'_M = \omega'_M + \left(\alpha_1^M - \alpha_0^M\right)^2\lambda_v^M/\hbar$ is the renormalized vibrational frequency when the monomer is in the electronic excited state. The factor $\vec{\mu}_{M'}$ denotes the transition dipole moment for the $0 \rightarrow 1$ transition for the vibration on site M, on the electronic excited state. Aside from the increased complexity of the third-order lineshape functions, which are described in detail for the general case in Appendix A, the main difference from the ground state pathways is in the transition dipole term, with the replacement of, *e.g.*, $|\vec{\mu}_M|^2$ with $|\vec{\mu}_{M'}U_{\beta M}|^2$, the transition dipole for the vibration on site M when exciton $|\beta\rangle$ is populated. The origin of the two terms can be understood from Figure 1. The first term is related to the probability that the monomer M is in the electronic excited state, whereas the second term is related to the probability that it is in the electronic ground state. The factor of $U_{\beta M}$ is the fraction of exciton $|\beta\rangle$ that is localized on site M. For the case of the dimer, it is simply related to the mixing angle, *e.g.*, as either $U_{\mu A} = \cos\theta$ or $U_{\nu A} = -\sin\theta$. This additional factor scales the signal with the probability that the electronic excitation is localized on a given site and is a crucial piece of information that impacts the 2DEV spectra much more directly than other techniques, such as 2DES.

We assume for this work that the interaction with the infrared pulse will only drive vibrational transitions, neglecting the possibility that it will excite transitions between the excitons. For the small excitonic energy gaps considered here,

such transitions would appear at a much lower frequency (~200 cm^{-1}) than the vibrational transitions (~1500 cm^{-1}). A combined excitation of a vibration together with the excitonic transition will, however, have a similar energy to the pure vibrational transition, but these transitions might be very weak, depending on the symmetries and selection rules for the vibrations. For large polyatomic molecules, these selection rules can become very complex.[45–47] In either case, the electronic coherences will typically dephase much more quickly than the vibrational coherences, and so, the resulting features are expected to be broad and structureless.

The frequency domain 2DEV spectrum is computed in the impulsive limit by taking the Fourier transform over the t_1 and t_3 domains for each term in the response function. The total response is then given by the sum of the rephasing and nonrephasing components as $S^{tot}(\omega_1,t_2,\omega_3) = S^R(-\omega_1,t_2,\omega_3) + S^{NR}(\omega_1,t_2,\omega_3)$. The rephasing component is reflected along the ω_1 axis because of the change in the sign of the t_1 coherence oscillation term between the rephasing and nonrephasing pathways. The purely absorptive spectrum corresponds to the real part of the total spectrum, so the final result is given by $S^{abp} = \mathrm{Re}\,[S^{tot}]$. To relax the impulsive approximation, the response functions should be convolved with the electromagnetic fields prior to the Fourier transforms. So long as the spectral bandwidths of the fields are sufficient to cover all of the transitions of interest and the pulse durations are significantly shorter than the time scale of the exciton dynamics, inclusion of realistic laser pulses should not significantly alter the discussion of the current work, so for simplicity, we do not account for this additional experimental complication.

The response function method used in this work does not provide the exact result, primarily due to the neglect of the exciton coupling terms in the Hamiltonian, as described following Equation (9), but it has substantial benefits in the ease of interpretation. With the response functions, it is easy to consider the results term-by-term, and so, there is no doubt as to the origin or interpretation of any given feature. It would certainly be possible to simulate the spectral response using an exact method for solving the quantum dynamics, such as the hierarchy equations of motion,[35,48,49] but for establishing the feasibility of our proposed approach, the current method should prove adequate.

III. SIMULATION RESULTS

A series of 2DEV spectra calculated using this model are shown in Figure 3 for two different strengths of the electronic coupling J, where we have chosen $J = -50$ cm^{-1} and

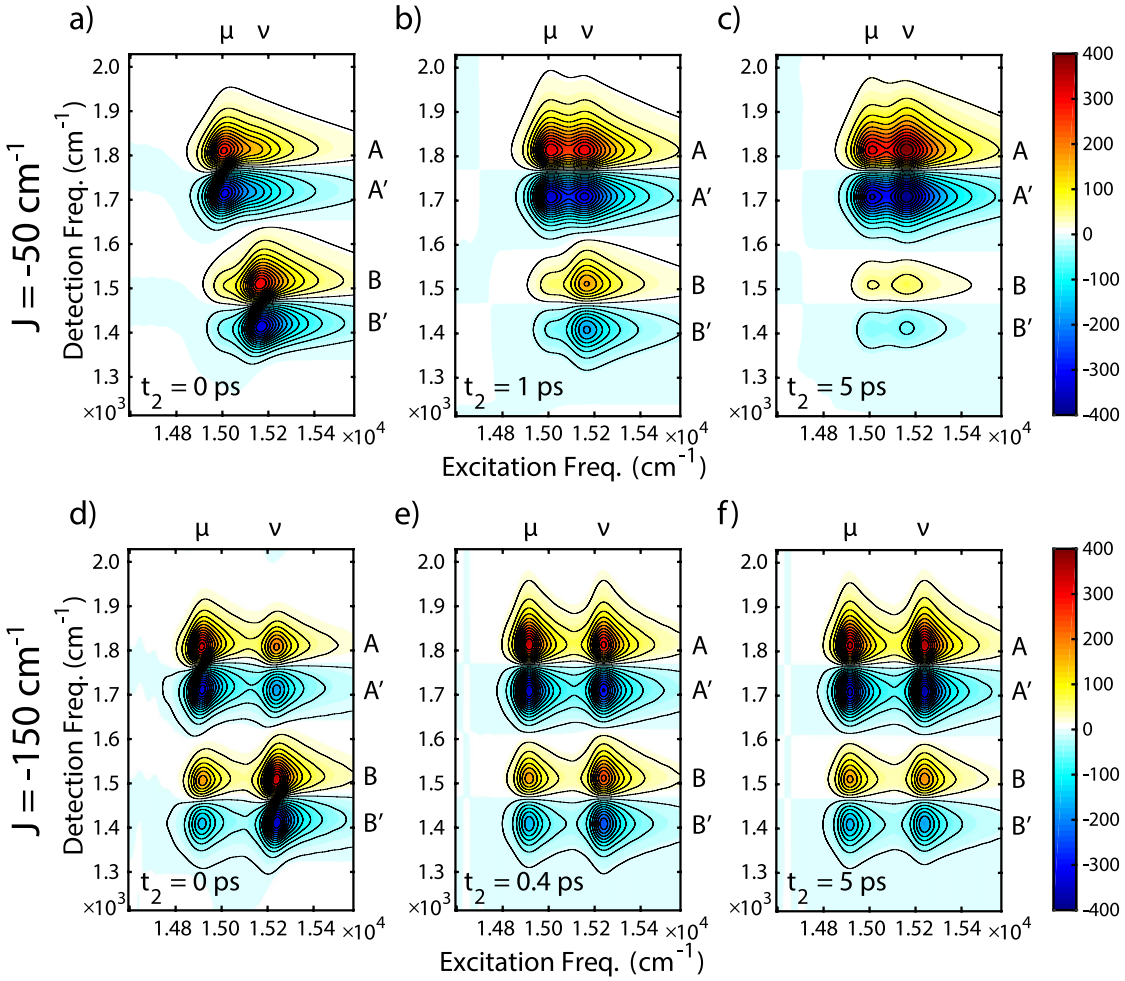

FIG. 3. 2DEV spectra for an electronic coupling of $J = -50$ cm^{-1} at (a) $t_2 = 0$ ps, (b) $t_2 = 1$ ps, and (c) $t_2 = 5$ ps, and for an electronic coupling of $J = -150$ cm^{-1} at (d) $t_2 = 0$ ps, (e) $t_2 = 0.4$ ps, and (f) $t_2 = 5$ ps. The excitons and vibrations are labelled for clarity. The rest of the parameters used in these simulations are provided in the text.

-150 cm^{-1}. The spectra are shown at several different waiting times following the initial excitation, to demonstrate the structure of the spectra that result from our model. For these simulations, the site energy difference was $\epsilon_B - \epsilon_A = 125$ cm^{-1}, and the vibrational frequencies were set to $\omega_A = 1800$ cm^{-1}, $\omega'_A = 1700$ cm^{-1}, $\omega_B = 1500$ cm^{-1}, and $\omega'_B = 1400$ cm^{-1}. These values for the frequencies were chosen to be similar to a C=C or C=O double bond stretch, as these types of modes are common in organic chromophores and have been studied in previous transient infrared experiments of light-harvesting complexes.[26,27,50] The spectral densities for the baths were taken to have the Drude-Lorentz form,

$$\mathcal{J}_x^M(\omega) = \frac{2\lambda_x^M \omega_{c_x}{}^M \omega}{\omega_{c_x}{}^{M2} + \omega^2}, \tag{16}$$

with reorganization energies set to $\lambda_e^A = \lambda_e^B = 35$ cm^{-1} and $\lambda_v^A = \lambda_v^B = 5$ cm^{-1} and cutoff frequencies for the time scales of the baths were set to $\omega_{c_e}{}^A = \omega_{c_e}{}^B = \omega_{c_v}{}^A = \omega_{c_v}{}^B = 50$ cm^{-1}. We have chosen the parameters α_0 and α_1 for both monomers to take on the values 0.6 and 1.6, respectively, so that the vibrational transition on the electronic excited state couples to the bath with the same overall strength as the vibrational transition on the ground electronic state. The magnitude of these parameters is comparable to those found in measurements on the laser dye 3,3′-diethylthiatricarbocyanine iodide (DTTCI) in chloroform.[31] The temperature was set to $T = 77$ K, as most multidimensional spectroscopy experiments on photosynthetic pigment-protein complexes are performed at this temperature, to improve the resolution of overlapping excitonic states. At $T = 300$ K for the current parameters, the features become broad and unresolvable (results not shown). The bath parameters were chosen to be similar to those typically found in photosynthetic pigment-protein complexes.[51,52] For demonstrative purposes, the transition dipole moments were all set to 1, and the electronic transition dipole moments for the monomers were assumed to be perpendicular. We will demonstrate in Section IV how these parameters can be removed in the extraction of the electronic site populations, and so, this choice does not affect the results.

In each of the spectra shown in Figure 3, there are four positive-going features that correspond to probing vibrations on the ground electronic state, and four negative-going features that correspond to vibrations on the electronic excited states (see Figure 2). The features arise from each combination of exciton and vibrational mode, and the intensity of a given feature is proportional to the probability that the electronic excitation is localized on that monomer, together with the associated transition dipole moments. As t_2 increases, the intensities of the features change, with those features corresponding to probing site A (the lower energy site) increasing and those corresponding to probing site B (the higher energy site) decreasing, due to the relaxation of the electronic populations towards thermal equilibrium. Comparing the simulations with different strengths of electronic coupling, for the stronger coupling case, the exciton absorption energies show a greater separation, due to the larger splitting between the excitonic energies. Furthermore, the intensities of the features resulting from probing the separate monomers are more similar, due to the greater delocalization of the excitons relative to the weaker coupling case. Both traits are directly related to the formation of delocalized excitonic states by the electronic coupling.

The 2DEV spectrum reports on the exciton that is initially populated, but otherwise, it does not provide direct information on the electronic state of the system. Instead, it provides information relating to the spatial distribution of the electronic excitation. As the higher energy exciton $|\nu\rangle$ relaxes and the population is transferred to $|\mu\rangle$, the ratio between the peaks corresponding to exciting $|\nu\rangle$ and probing the vibrations on sites A and B becomes more like the ratio of site populations for exciton $|\mu\rangle$. At long waiting times, the spectra reflect the thermal populations of electronic excited states. For the low temperature simulations shown here, the equilibrium population of the higher energy exciton is very small, and, whether $|\mu\rangle$ or $|\nu\rangle$ is initially excited, the long-time ratios between the monomer A and B features are very similar to the ratio for the lower energy exciton.

There is no difference between the dynamics obtained by probing the vibrations when the monomer is on either the ground or the excited electronic state. In each case, the dynamics originate from the pathways $R_{\alpha\beta M'}$, where the system evolves according to the electronic excited state. From Equations (14), (15), (B1), and (B2), the amplitudes resulting from these pathways depend on the probability that a given exciton is populated, together with the fraction of that exciton localized on each monomer. These features suggest that it should be possible to directly extract the electronic site populations from the spectra, without the need for a model. A method for isolating this information is described in Section IV.

In addition to reporting on the dynamics of the system during the waiting time, the 2DEV spectra also provide information about the bath dynamics and the system-bath coupling. At early waiting times, the features in the 2DEV spectra have positive center-line slopes, which is indicative of the initial correlation between the electronic and vibrational transition frequencies. For the isolated monomers, the decay of this slope is proportional to the correlation function for the bath-induced fluctuations in the energy of the vibrational transition, and there may be a long-time non-zero slope when there exists a correlation between the inhomogeneous distributions of the electronic and vibrational energy gaps.[30,31] Due to the electronic mixing in the dimer, the specific form of the center-line slope becomes more complicated, as it will contain contributions from multiple pathways and will depend on the electronic mixing angle and the correlation functions for the vibration on each monomer. The dynamics still reflect the correlation between the electronic and vibrational transitions, primarily induced via the fluctuations of the vibrational zero-point energies on the electronic excited state, but interference effects may complicate the precise dynamics.[37,38] A detailed analysis of the information that can be extracted from these slopes is left for future considerations.

IV. MEASUREMENT OF ELECTRONIC SITE POPULATIONS

The major advantage of 2DEV comes from its ability to provide a direct experimental connection between the electronic eigenstates and the physical location of the excitation

energy on a molecular scale. In this section, we demonstrate how the 2DEV spectrum of a molecular aggregate could be used to directly measure the electronic site populations. As will become clear, this method does not rely on a model. The fundamental experimentally measurable quantity that we use is $S_{\alpha M}(t_2)$, the integrated intensity of the spectral feature arising from excitation of exciton $|\alpha\rangle$ and detection of the vibration on site M. We can choose to use the features that arise from probing the vibration on either the electronic ground or excited state, each of which contains contributions from the pathways $R_{\alpha\beta M'}$. For probing the vibration on the electronic ground state, this is given by

$$\begin{aligned} S_{\alpha M}(t_2) &= \int \mathrm{d}\omega_1 \mathrm{d}\omega_3 \sum_{\beta} S^{abp}_{\alpha\beta M}(\omega_1, t_2, \omega_3) \\ &= \left\langle |\vec{\mu}_\alpha|^2 |\vec{\mu}_M|^2 \right\rangle P_{\alpha M}(t_2), \end{aligned} \tag{17}$$

where $P_{\alpha M}(t_2)$ is the probability that the electronic excitation is localized on site M at time t_2, given that the initial excitation populated exciton $|\alpha\rangle$. The sum runs over all the exciton states. The only change that is made for probing the vibration on the electronic excited state is to replace the vibrational transition dipole on the electronic ground state, $|\vec{\mu}_M|^2$, with that on the electronic excited state, $|\vec{\mu}_{M'}|^2$. The overall probability that an electronic excited state is populated at time t_2, following excitation to exciton $|\alpha\rangle$, is given by $\sum_N P_{\alpha N}(t_2)$, so the normalized site population is given by

$$\begin{aligned} \frac{P_{\alpha M}(t_2)}{\sum_N P_{\alpha N}(t_2)} &= \left(1 + \sum_{N \neq M} \frac{P_{\alpha N}(t_2)}{P_{\alpha M}(t_2)}\right)^{-1} \\ &= \left(1 + \sum_{N \neq M} \frac{\left\langle |\vec{\mu}_M|^2 \right\rangle}{\left\langle |\vec{\mu}_N|^2 \right\rangle} \frac{S_{\alpha N}(t_2)}{S_{\alpha M}(t_2)}\right)^{-1}. \end{aligned} \tag{18}$$

The only information required in addition to the 2DEV spectral amplitudes is therefore the ratios of transition dipole moments for the vibrations on either the electronic ground or excited state, depending on which features are being used. It is also important to note that any decay of the signal due to relaxation to the electronic ground state will be removed by the normalization. If it is desired that the relaxation to the ground electronic state be included, then Equation (18) must be modified by taking the denominator on the left-hand side at $t_2 = 0$. This, however, may introduce difficulties related to the finite duration of real laser pulses.

So far as the current discussion is concerned, there is no significant difference between the information content that can be extracted from probing the vibrations on the ground versus the excited electronic states. This choice is a practical matter, since in particular molecules and for particular vibrations, the vibrational transition dipoles on the ground and excited electronic states might have very different magnitudes. For example, 2DEV spectra of the C=C backbone stretch mode in DTTCI are dominated by the electronic ground state feature,[31] whereas in 8′-apo-β-caroten-8′-al, the spectrum is dominated by electronic excited state features.[53,54] Additionally, it is often easier to assign vibrations on the ground electronic state, due to the computational expense of *ab initio* excited state frequency analysis.

There is, however, a substantial difference in the ease with which the ratio of vibrational transition dipoles that appears in Equation (18) can be measured for the ground or excited electronic states. For the ground electronic state, this ratio can be easily extracted from the vibrational linear absorption. The ratio $\left\langle |\vec{\mu}_{M'}|^2 \right\rangle / \left\langle |\vec{\mu}_{N'}|^2 \right\rangle$ between vibrational transition dipoles on the electronic excited state, however, is, in general, very difficult to measure. In principle, it could be extracted from transient-2DIR spectra, or approximated from the 2DEV spectra of the monomers in isolation, but each of these approaches would require performing another difficult experiment in addition to measuring the 2DEV spectra of the system of interest. Here, we propose a method for measuring this ratio that requires only the 2DEV spectrum at $t_2 = 0$ and the electronic linear absorption spectrum. To understand this procedure, consider $S^{(1)}_\alpha$, the integrated intensity of the electronic linear absorption to exciton $|\alpha\rangle$. This is given by

$$S^{(1)}_\alpha = \int \mathrm{d}\omega \left\langle |\vec{\mu}_\alpha|^2 \right\rangle S^{(1)}_\alpha(\omega) = \left\langle |\vec{\mu}_\alpha|^2 \right\rangle, \tag{19}$$

where $S^{(1)}_\alpha(\omega)$ is given by the Fourier Transform of the linear lineshape function $g_\alpha(t)$. This integrated intensity can be related to the integrated intensity of the 2DEV spectrum at $t_2 = 0$ as $S^{(1)}_\alpha = \sum_N S_{\alpha N}(0) / \left\langle |\vec{\mu}_{N'}|^2 \right\rangle$. Therefore, if we populate a vector $|S^{(1)}\rangle$ with the values $S^{(1)}_\alpha$ for every exciton $|\alpha\rangle$, and a matrix $\hat{S}_{ex-site}$ with the values $S_{\alpha N}(0)$ for every exciton $|\alpha\rangle$ and site N, then it is possible to extract the required ratio of transition dipoles as

$$\frac{\left\langle |\vec{\mu}_{M'}|^2 \right\rangle}{\left\langle |\vec{\mu}_{N'}|^2 \right\rangle} = \frac{\left\langle N \left| \hat{S}^{-1}_{ex-site} \right| S^{(1)} \right\rangle}{\left\langle M \left| \hat{S}^{-1}_{ex-site} \right| S^{(1)} \right\rangle}, \tag{20}$$

where $|N\rangle = |0_1, 0_2, \ldots, 0_{N-1}, 1_N, 0_{N+1}, \ldots\rangle$ indicates a unit vector representing site N. In Equation (20), the matrix $\hat{S}_{ex-site}$ can be thought of as a linear mapping between the exciton basis and the site basis. The special case of the dimer is given by

$$\frac{\left\langle |\vec{\mu}_{A'}|^2 \right\rangle}{\left\langle |\vec{\mu}_{N'}|^2 \right\rangle} = \frac{S^{(1)}_\mu S_{\nu A}(0) - S^{(1)}_\nu S_{\mu A}(0)}{S^{(1)}_\nu S_{\mu N}(0) - S^{(1)}_\mu S_{\nu N}(0)}, \tag{21}$$

where N is either site A or B. Therefore, so long as it is possible to measure $S_{\alpha N}(t_2)$ and $S^{(1)}_\alpha$ for each exciton $|\alpha\rangle$ and each site N, then it should be possible to isolate $P_{\alpha M}(t_2) / \sum_N P_{\alpha N}(t_2)$, the population on site M following excitation to exciton $|\alpha\rangle$ at time t_2. Note that in a real experiment with finite pulse durations, the spectrum at $t_2 = 0$ might be contaminated by other pathways, and so, Equation (20) becomes approximate, and it may be necessary to use a different method to estimate the ratio of transition dipoles.

Once the relevant ratio of vibrational transition dipole moments has been measured, the only information necessary from the 2DEV spectrum to extract the site populations following excitation to exciton $|\alpha\rangle$ is the quantity $S_{\alpha M}(t_2)$, for each site M. This might be a very difficult task in a real situation, when there are many vibrational transitions and many excitons, all potentially overlapping in the spectrum. In the case shown in Figures 3(d)-3(f) with electronic coupling $J = -150$ cm^{-1}, it is relatively easy to see that this would be possible, due to the substantial splitting between the exciton energies. For the

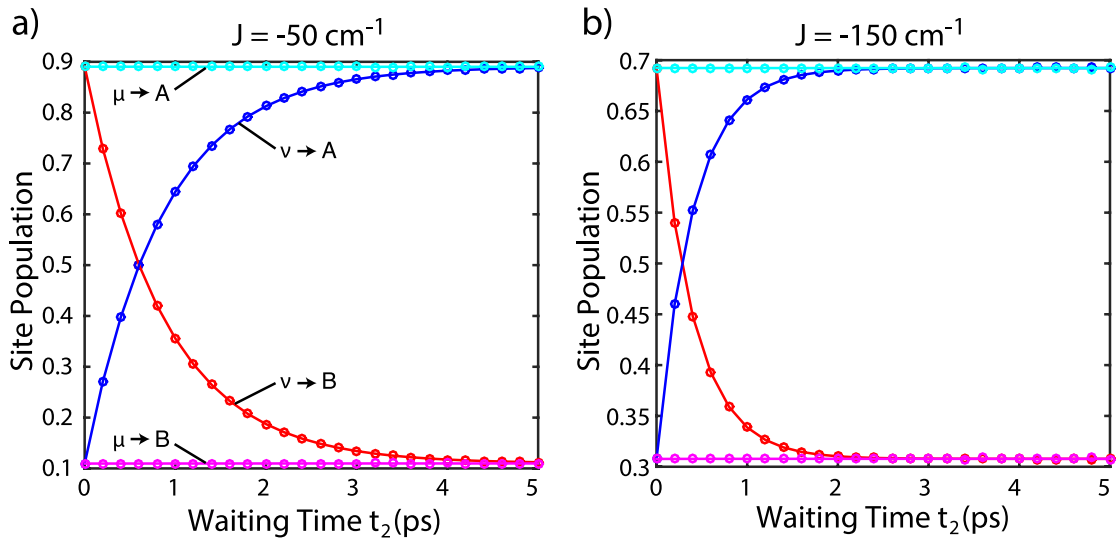

FIG. 4. The site populations extracted from the simulated spectra (circles), compared against the populations calculated by integrating the Redfield master equation (lines). The parameters are the same as for Figure 3. Panel (a) shows results for $J = -50$ cm^{-1}, and panel (b) shows results for $J = -150$ cm^{-1}. The blue and red curves show the populations on sites A and B following initial excitation to the higher energy exciton, while for the cyan and magenta curves, the initial excitation was to the lower energy exciton. For this figure, the values from the spectral simulations were taken from the electronic excited state features. It makes no difference if the ground state features are used instead.

weaker electronic coupling of $J = -50$ cm^{-1} shown in Figures 3(a)-3(c), the features corresponding to different excitons overlap significantly, and the separation of the contributions from each feature becomes more difficult. In many cases, even this degree of spectral resolution might not be possible. For experimental data, one method for extracting the necessary information and removing the interference from neighboring features might be to perform an evolution-associated decomposition of the spectrum.[55–57] In principle, however, Equation (18) provides a method by which the site population could be directly extracted from the experimental data without the need for a model Hamiltonian to relate the excitons to the sites.

A numerical demonstration of this procedure is shown in Figure 4. We take advantage of the fact that each term of the total response function is calculated separately, and so, it is trivial to calculate the integral over each individual contribution. In this figure, we compare the site populations as extracted from the simulations of the 2DEV spectra using Equation (18) with those calculated directly by propagating the Redfield master equations under the secular approximation. For the Redfield dynamical simulations, the initial conditions were chosen as either $\rho(0) = |\mu\rangle\langle\mu|$ or $|\nu\rangle\langle\nu|$. The results from the spectral simulations match perfectly with the results from the secular Redfield theory, demonstrating that there is no approximation in Equation (18). Furthermore, this method of extracting populations is not specific to the use of secular Redfield theory for the dynamics, and we expect that it should work equally well for exact quantum dynamics, or to extract the true quantum dynamics from the real experimental data. Therefore, this method provides a means by which 2DEV spectra can be used to directly extract the electronic site population as a function of time without need for a model, or the associated approximations. To our knowledge, no other experiment is currently capable of this measurement.

A schematic summary of the proposed method for extracting the electronic site populations from the 2DEV spectra is shown in Figure 5. The choice to use either the ground or excited electronic state features can be made based on convenience, and it makes only a practical difference. The only information required in addition to the 2DEV spectra is the ratio of vibrational transition dipoles, and no comparison with a model is necessary.

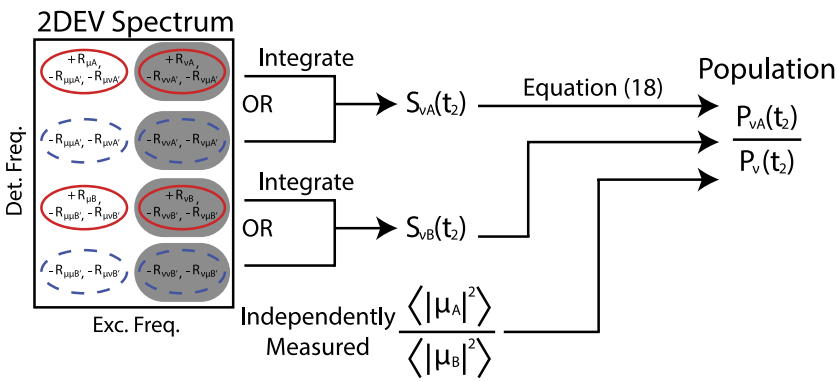

FIG. 5. A schematic overview of the proposed method for measuring the electronic site populations for a dimer. Either the ground or excited electronic state features are chosen for the analysis. The ratio of transition dipole moments for the vibrations on the relevant electronic state can be measured with any method, though some suggestions that rely only on linear absorption and the 2DEV spectrum are described in the text.

V. CONCLUSION

In this work, we have derived response functions for simulating the 2DEV spectra of a molecular dimer, and proposed a method by which the 2DEV spectra of a molecular aggregate could be used to directly measure the electronic site populations following the initial electronic excitation, without the need for a model to interpret the results. The proposed method, given by Equation (18) and illustrated schematically in Figure 5, makes no approximations that are apparent with the current model. To demonstrate the feasibility of this experiment, we have analyzed the results from the response function simulations that use excitonic dynamics consistent with Redfield theory, under the secular approximation, and compared the results with a direct quantum dynamics simulation. We believe that the results do not depend on the specific quantum dynamics used, and, in future work, we intend to demonstrate this, as well as relax some of the assumptions in the model. Of significant interest would be the direct measurement of coherent electronic dynamics, and the incorporation of vibronic mixing between the sites, involving either the probed vibration or a separate low frequency mode.[7,11,34,35] A number of synthetic and biological dimers which sample different parameter regimes have been described, which would serve as very interesting systems to test the practical application of this experiment.[58–65]

It is important to note that there are a number of practical difficulties that might limit the general applicability of the approach described in this work. In particular, it crucially relies on the ability to resolve the spectral features corresponding to each exciton and to a vibration on each site in the 2DEV spectra. For many commonly studied molecular aggregates, including J-aggregates and most photosynthetic pigment-protein complexes, this may be a difficult task. It is exacerbated by the absence of strong rephasing power in 2DEV spectroscopy, which means that the homogeneous and inhomogeneous components of the linewidth cannot be separated onto different axes, as occurs with degenerate techniques such as 2DES and 2DIR. This implies that unless the features can be resolved in the linear absorption spectra, it is unlikely that they will be resolvable in the 2DEV spectra. A possible approach to alleviating this difficulty might be to use an evolution-associated spectral decomposition, to take advantage of the different dynamics for each exciton and site, but this approach can be complicated and is not always guaranteed to provide all of the information required here. We expect that future experimental and theoretical studies will provide a method that is more generally applicable and robust to the complexity of real experimental systems.

Aside from these limitations, the promise of the proposed experiment is substantial. It represents, to our knowledge, the first experimental technique that directly links the energetic dynamics of electronic excitations with spatial information describing where in the complex the excitation is located, on the scale of individual pigments. Other experiments, such as time resolved fluorescence or transient absorption anisotropy,[66–68] 2DES with polarization control,[19,20] and coherent nonlinear frequency generation,[69] can provide indirect information which, when assisted by a model, can inform our understanding of the link between the excitonic and spatial structures, but they will always be strongly dependent on the details and quality of the model. 2DEV is capable of providing a direct experimental link between these representations and shows promise in aiding the development of a more complete picture of excitonic dynamics in molecular aggregates.

ACKNOWLEDGMENTS

This work was supported by the Director, Office of Science, Office of Basic Energy Sciences, U.S. Department of Energy under Contract No. DE-AC02-05CH11231, and the Division of Chemical Sciences, Geosciences and Biosciences Division, Office of Basic Energy Sciences through Grant No. DE-AC03-76F000098 (at Lawrence Berkeley National Laboratory and University of California, Berkeley). Additionally, this work used resources of the National Energy Research Scientific Computing Center, a DOE Office of Science User Facility supported by the Office of Science of the U.S. Department of Energy under Contract No. DE-AC02-05CH11231.

APPENDIX A: DERIVATION OF THE RESPONSE FUNCTIONS

Generic Feynman diagrams for the type of pathway considered in this work to describe the excited state dynamics are shown in Figure 6. The derivations in this section do not depend on any specific details of the system, so the labels $a - f$ are used to denote any generic states. The central approximation we are making here is that the energy transfer dynamics are determined by a rate $k_{c\leftarrow b}$ from $|b\rangle\langle b|$ to $|c\rangle\langle c|$, and a rate $k_{b\leftarrow c}$ for the reverse process, while assuming that there is no transfer between these populations and the coherences, e.g., $|b\rangle\langle b|$ to $|b\rangle\langle c|$. If we take the rates from the Redfield theory, then this corresponds to the secular approximation. It is important here because it allows us to write a relatively simple closed form for the response function. The substantial simplification allowed by this approximation appears if we notice that the overall nuclear propagator during t_2 has no contribution when isolated, and so when we perform the second order cumulant expansion, we will only have to consider the cross terms between t_1 and t_2 and between t_2 and t_3. The terms in the expansion that only depend on t_2 all cancel.

The response functions shown in Figure 6 can be written as[37,38]

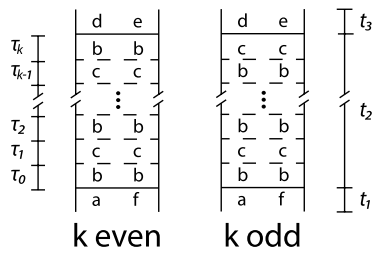

FIG. 6. Generic Feynman diagrams for the type of exciton dynamics considered in this work. During t_2, we allow k transitions between the population states in the one exciton manifold obeying some rate equation, with no coupling into coherences.

$$F(t_1,t_2,t_3;\{\tau_m\}) = \left\langle \mathcal{G}_{de,de}(t_3)\left[\prod_{m=0}^{k}\left(\delta_{me}\mathcal{G}_{bb,bb}(\tau_m)+\delta_{mo}\mathcal{G}_{cc,cc}(\tau_m)\right)\right]\mathcal{G}_{af,af}(t_1)\rho_{eq}\right\rangle, \tag{A1}$$

where ρ_{eq} is the equilibrium density matrix, $\mathcal{G}_{ij,ij}(t)$ denotes the Liouville space Green's function that describes evolution according to the state $|i\rangle\langle j|$, and δ_{me} and δ_{mo} are delta functions that test for whether m is even or odd, respectively.

Written in terms of the Hilbert space time evolution operators, we have

$$\begin{aligned}
F(t_1,t_2,t_3;\{\tau_m\}) = \Bigg\langle & \exp_-\left(\frac{i}{\hbar}\int_0^{t_1} d\tau' U_{fg}\right)\exp_-\left(\frac{i}{\hbar}\int_{t_1}^{t_1+\tau_0} d\tau' U_{bg}\right)\times\left[\prod_{m=0}^{k-1}\exp_-\left(\frac{i}{\hbar}\int_{t_1+\sum_{n=0}^{m}\tau_n}^{t_1+\sum_{n=0}^{m+1}\tau_n} d\tau'_m\left(U_{cg}\delta_{me}+U_{bg}\delta_{mo}\right)\right)\right] \\
& \times\exp_-\left(\frac{i}{\hbar}\int_{t_1+t_2}^{t_1+t_2+t_3} d\tau' U_{eg}\right)\exp_+\left(-\frac{i}{\hbar}\int_{t_1+t_2}^{t_1+t_2+t_3} d\tau' U_{dg}\right) \\
& \times\left[\prod_{m=0}^{k-1}\exp_+\left(-\frac{i}{\hbar}\int_{t_1+\sum_{n=0}^{m}\tau_n}^{t_1+\sum_{n=0}^{m+1}\tau_n} d\tau'_m\left(U_{cg}\delta_{me}+U_{bg}\delta_{mo}\right)\right)\right] \\
& \times\exp_+\left(-\frac{i}{\hbar}\int_{t_1}^{t_1+\tau_0} d\tau' U_{bg}\right)\exp_+\left(-\frac{i}{\hbar}\int_0^{t_1} d\tau' U_{ag}\right)\rho_{eq}\Bigg\rangle,
\end{aligned} \tag{A2}$$

where $\exp_+$ and $\exp_-$ are, respectively, the positively and negatively time-ordered exponentials, and $U_{ig} = \left(V_i - V_g\right) - \left\langle V_i - V_g\right\rangle$ denotes the difference between the system-bath coupling terms in the Hamiltonian for level $|i\rangle$ and the ground state.[43,44] Now, via an application of the second order cumulant expansion, we can find the general result for the third order lineshape function to be

$$F(t_1,t_2,t_3;\{\tau_m\}) = \mathcal{F}(t_1,t_2,t_3)\times\mathfrak{F}(t_2,t_3,\{\tau_m\}), \tag{A3}$$

where the part that depends on the initial and final states, but not on the specific trajectory, is

$$\begin{aligned}
\mathcal{F}(t_1,t_2,t_3) = & \exp\left[-g_{dd}(t_3)-g^*_{ee}(t_3)-g_{aa}(t_1)-g^*_{ff}(t_1)\right]\times\exp\left[-f^-_{da}(t_1,t_2,t_3)+f^{-\,*}_{df}(t_1,t_2,t_3)+2\,\mathrm{Re}\left[g_{de}(t_3)\right]\right] \\
& \times\exp\left[2\,\mathrm{Re}\left[g_{af}(t_1)\right]+f^-_{ae}(t_1,t_2,t_3)-f^{-\,*}_{fe}(t_1,t_2,t_3)\right]
\end{aligned} \tag{A4}$$

with the auxiliary lineshape function

$$f^-_{ij}(t_1,t_2,t_3) = g_{ij}(t_2)-g_{ij}(t_1+t_2)-g_{ij}(t_2+t_3)+g_{ij}(t_1+t_2+t_3). \tag{A5}$$

The part that depends on details of the particular trajectory is

$$\begin{aligned}
\mathfrak{F}(t_2,t_3,\{\tau_m\}) = & \times\exp\left[2i\,\mathrm{Im}\left[g_{be}(t_2+t_3)-g_{be}(t_2+t_3-\tau_0)-g_{be}(t_2)+g_{be}(t_2-\tau_0)\right]\right] \\
& \times\exp\left[2i\sum_{m=0}^{k-1}\delta_{mo}\,\mathrm{Im}\left[g_{be}\left(t_2+t_3-\sum_{n=0}^{m}\tau_n\right)-g_{be}\left(t_2+t_3-\sum_{n=0}^{m+1}\tau_n\right)-g_{be}\left(t_2-\sum_{n=0}^{m}\tau_n\right)+g_{be}\left(t_2-\sum_{n=0}^{m+1}\tau_n\right)\right]\right] \\
& \times\exp\left[2i\sum_{m=0}^{k-1}\delta_{me}\,\mathrm{Im}\left[g_{ce}\left(t_2+t_3-\sum_{n=0}^{m}\tau_n\right)-g_{ce}\left(t_2+t_3-\sum_{n=0}^{m+1}\tau_n\right)-g_{ce}\left(t_2-\sum_{n=0}^{m}\tau_n\right)+g_{ce}\left(t_2-\sum_{n=0}^{m+1}\tau_n\right)\right]\right] \\
& \times\exp\left[-2i\,\mathrm{Im}\left[g_{bd}(t_2+t_3)-g_{bd}(t_2+t_3-\tau_0)-g_{bd}(t_2)+g_{bd}(t_2-\tau_0)\right]\right] \\
& \times\exp\left[-2i\sum_{m=0}^{k-1}\delta_{mo}\,\mathrm{Im}\left[g_{bd}\left(t_2+t_3-\sum_{n=0}^{m}\tau_n\right)-g_{bd}\left(t_2+t_3-\sum_{n=0}^{m+1}\tau_n\right)-g_{bd}\left(t_2-\sum_{n=0}^{m}\tau_n\right)+g_{bd}\left(t_2-\sum_{n=0}^{m+1}\tau_n\right)\right]\right] \\
& \times\exp\left[-2i\sum_{m=0}^{k-1}\delta_{me}\,\mathrm{Im}\left[g_{cd}\left(t_2+t_3-\sum_{n=0}^{m}\tau_n\right)-g_{cd}\left(t_2+t_3-\sum_{n=0}^{m+1}\tau_n\right)-g_{cd}\left(t_2-\sum_{n=0}^{m}\tau_n\right)+g_{cd}\left(t_2-\sum_{n=0}^{m+1}\tau_n\right)\right]\right].
\end{aligned} \tag{A6}$$

Here, we define the lineshape functions

$$\begin{aligned}
g_{ij}(t) &= \int_0^t d\tau_1\int_0^{\tau_1} d\tau_2\, C_{ij}(\tau_2), \\
C_{ij}(t) &= \frac{1}{\hbar^2}\left\langle U_{ig}(t)U_{jg}(0)\rho_{eq}\right\rangle,
\end{aligned} \tag{A7}$$

where the angular brackets indicate averaging over the bath coordinates. Note that for any given pathway, either a or f is the ground state, so many of the terms in the above equation will not contribute (note that $U_{gg}(t) = 0$). Typically, there will also be some relation between d and e that will result in simplification, as well.

To calculate the total response, it is necessary to integrate the above equation over all possible trajectories for a fixed t_2. The probability of a specific trajectory that has k transitions during t_2 and begins on state $|b\rangle\langle b|$ is given by

$$P_b(k,t_2,\{\tau_m\}) = \Theta\left(t_2 - \sum_{m=0}^{k-1}\tau_m\right)\left(\delta_{ke}(k_{c\leftarrow b}\,k_{b\leftarrow c})^{\frac{k}{2}} + \delta_{ko}\left(k_{c\leftarrow b}^{\frac{k+1}{2}}\,k_{b\leftarrow c}^{\frac{k-1}{2}}\right)\right)$$
$$\times \exp\left[-\left(k_{c\leftarrow b}\delta_{ke} + k_{b\leftarrow c}\delta_{ko}\right)\left(t_2 - \sum_{m=0}^{k-1}\tau_m\right)\right]\prod_{m=0}^{k-1}\exp\left[-\left(k_{c\leftarrow b}\delta_{me} + k_{b\leftarrow c}\delta_{mo}\right)\tau_m\right], \tag{A8}$$

where $\Theta(t)$ denotes a Heaviside step function. The overall response function is then given by

$$F(t_1,t_2,t_3) = \sum_{k=0}^{\infty}\int_0^{t_2} d\tau_0 \int_0^{t_2} d\tau_1 \ldots \int_0^{t_2} d\tau_{k-1}\, P_b\left(k,t_2,\{\tau_m\}\right)\, F(t_1,t_2,t_3;\{\tau_m\}). \tag{A9}$$

To calculate a specific term of the response function, it is necessary to split up Equation (A9) in terms of the final state, which gives us the final result,

$$F_{bb}(t_1,t_2,t_3) = \sum_{k=0}^{\infty}\int_0^{t_2} d\tau_0 \int_0^{t_2} d\tau_1 \ldots \int_0^{t_2} d\tau_{k-1}\,\delta_{ke}\, P_b\left(k,t_2,\{\tau_m\}\right)\, F(t_1,t_2,t_3;\{\tau_m\}), \tag{A10}$$

$$F_{bc}(t_1,t_2,t_3) = \sum_{k=0}^{\infty}\int_0^{t_2} d\tau_0 \int_0^{t_2} d\tau_1 \ldots \int_0^{t_2} d\tau_{k-1}\,\delta_{ko}\, P_b\left(k,t_2,\{\tau_m\}\right)\, F(t_1,t_2,t_3;\{\tau_m\}). \tag{A11}$$

In practice, these summations can be truncated after a finite number of terms, as for a given t_2, the probability of a trajectory approaches 0 for large values of k. This can be clearly seen when it is recognized that Equation (A8) reduces to a Poisson distribution when $k_{c\leftarrow b} = k_{b\leftarrow c}$. For the simulations in this work, the multidimensional integrals were computed using the VEGAS Monte Carlo algorithm,[70] and it was typically sufficient to truncate the summation to fewer than 10 terms.

APPENDIX B: EQUIVALENCE WITH SECULAR REDFIELD

We can verify that the dynamics used in the spectral simulations are the same as for secular Redfield theory, with the initial conditions of $\rho(0) = |\mu\rangle\langle\mu|$ or $\rho(0) = |\nu\rangle\langle\nu|$. For the spectral simulations, the dynamics following excitation of exciton $|\mu\rangle$ are given by the direct integration of equations

$$\rho_{\mu\leftarrow\mu}(t) = \sum_{k=0}^{\infty}\int_0^{t} d\tau_0 \int_0^{t} d\tau_1 \ldots \int_0^{t} d\tau_k\,\delta_{ke}\, P_\mu\left(k,t,\{\tau_i\}\right) \tag{B1}$$

and

$$\rho_{\nu\leftarrow\mu}(t) = \sum_{k=0}^{\infty}\int_0^{t} d\tau_0 \int_0^{t} d\tau_1 \ldots \int_0^{t} d\tau_k\,\delta_{ko}\, P_\mu\left(k,t,\{\tau_i\}\right) \tag{B2}$$

with analogous equations for the initial condition $\rho(0) = |\nu\rangle\langle\nu|$.

To show that the secular Redfield dynamics are equivalent to the dynamics from Equations (B1) and (B2), we can write the formal solution to the Redfield equations in the interaction picture,[42]

$$\rho_{\alpha\beta} = \rho_{\alpha\beta}(0)e^{\mathcal{R}_{\alpha\beta,\gamma\delta}t} + \sum_{(\gamma,\delta)\neq(\alpha,\beta)}\mathcal{R}_{\alpha\beta,\gamma\delta}\int_0^{t} dt' e^{\mathcal{R}_{\alpha\beta,\alpha\beta}(t-t')}e^{i(\omega_{\alpha\beta}-\omega_{\gamma\delta})t'}\rho_{\gamma\delta}(t'). \tag{B3}$$

Now we will make the secular approximation and focus on the population dynamics of the dimer system, and take the initial condition to be $\rho_{\mu\mu}(0) = 1$. Under these conditions, we can find the population terms for the singly excited states to be

$$\begin{aligned}\rho_{\mu\mu}(t) &= e^{-\mathcal{R}_{\mu\mu,\mu\mu}(t)} + \mathcal{R}_{\mu\mu,\nu\nu}\int_0^{t} dt'\, e^{\mathcal{R}_{\mu\mu,\mu\mu}(t-t')}\rho_{\nu\nu}(t'),\\ \rho_{\nu\nu}(t) &= \mathcal{R}_{\nu\nu,\mu\mu}\int_0^{t} dt'\, e^{\mathcal{R}_{\nu\nu,\nu\nu}(t-t')}\rho_{\mu\mu}(t').\end{aligned} \tag{B4}$$

By combining these equations and making the identification of $k_{\nu\leftarrow\mu} = \mathcal{R}_{\mu\mu,\mu\mu} = -\mathcal{R}_{\nu\nu,\mu\mu}$ and $k_{\mu\leftarrow\nu} = \mathcal{R}_{\nu\nu,\nu\nu} = -\mathcal{R}_{\mu\mu,\nu\nu}$, we can get a recursive equation for $\rho_{\mu\mu}(t)$, which when taken to infinite depth becomes

$$\rho_{\mu\mu}(t) = \sum_{k'=0}^{\infty}\int_0^{t} dt'_0 \ldots \int_0^{t'_{2k-1}} dt'_{2k}\left(k_{\mu\leftarrow\nu}k_{\nu\leftarrow\mu}\right)^{k'}\prod_{i=0}^{2k'}\left(\exp\left[-(k_{\nu\leftarrow\mu}\delta_{ie} + k_{\mu\leftarrow\nu}\delta_{io})(t-t'_i)\right]\right) \tag{B5}$$

with an analogous equation for $\rho_{vv}(t)$. Under a straightforward change of variables, Equation (B5) is equivalent to Equation (B1). Therefore, the only approximation to the dynamics in the spectral simulations on top of those already made in the secular Redfield theory is the truncation of Equations (B1) and (B2) after a finite number of terms. This is acceptable because this sum can be made to converge to the limiting value with a moderate number of terms.

[1]G. D. Scholes, G. R. Fleming, A. Olaya-Castro, and R. van Grondelle, Nat. Chem. **3**, 763 (2011).
[2]H. van Amerongen, L. Valkunas, and R. van Grondelle, *Photosynthetic Excitons* (World Scientific, 2000).
[3]R. E. Blankenship, *Molecular Mechanisms of Photosynthesis* (Blackwell Publishing, 2002).
[4]N. S. Ginsberg, Y.-C. Cheng, and G. R. Fleming, Acc. Chem. Res. **42**, 1352 (2009).
[5]F. Milota, J. Sperling, A. Nemeth, T. Mancal, and H. F. Kauffmann, Acc. Chem. Res. **42**, 1364 (2009).
[6]H. Lee, Y.-C. Cheng, and G. R. Fleming, Science **316**, 1462 (2007).
[7]G. S. Engel, T. R. Calhoun, E. L. Read, T.-K. Ahn, T. Mancal, Y.-C. Cheng, R. E. Blankenship, and G. R. Fleming, Nature **446**, 782 (2007).
[8]A. Ishizaki and G. R. Fleming, Proc. Natl. Acad. Sci. U. S. A. **106**, 17255 (2009).
[9]P. Rebentrost, M. Mohseni, I. Kassal, S. Lloyd, and A. Aspuru-Guzik, New J. Phys. **11**, 033003 (2009).
[10]G. Panitchayangkoon, D. Hayes, K. A. Fransted, J. R. Caram, E. Harel, J. Wen, R. E. Blankenship, and G. S. Engel, Proc. Natl. Acad. Sci. U. S. A. **107**, 12766 (2010).
[11]E. Collini, C. Y. Wong, K. E. Wilk, P. M. G. Curmi, P. Brumer, and G. D. Scholes, Nature **463**, 644 (2010).
[12]G. Panitchayangkoon, D. V. Voronine, D. Abramavicius, J. R. Caram, N. H. C. Lewis, S. Mukamel, and G. S. Engel, Proc. Natl. Acad. Sci. U. S. A. **108**, 20908 (2011).
[13]E. Romero, R. Augulis, V. I. Novoderezhkin, M. Ferretti, J. Thieme, D. Zigmantas, and R. van Grondelle, Nat. Phys. **10**, 676 (2014).
[14]F. D. Fuller, J. Pan, A. Gelzinis, V. Butkus, S. S. Senlik, D. E. Wilcox, C. F. Yocum, L. Valkunas, D. Abramavicius, and J. P. Ogilvie, Nat. Chem. **6**, 706 (2014).
[15]J. Adolphs and T. Renger, Biophys. J. **91**, 2778 (2006).
[16]M. Cho, H. M. Vaswani, T. Brixner, J. Stenger, and G. R. Fleming, J. Phys. Chem. B **109**, 10542 (2005).
[17]T. R. Calhoun, N. S. Ginsberg, G. S. Schlau-Cohen, Y.-C. Cheng, M. Ballottari, R. Bassi, and G. R. Fleming, J. Phys. Chem. B **113**, 16291 (2009).
[18]D. Hayes and G. S. Engel, Biophys. J. **100**, 2043 (2011).
[19]G. S. Schlau-Cohen, T. R. Calhoun, N. S. Ginsberg, M. Ballottari, R. Bassi, and G. R. Fleming, Proc. Natl. Acad. Sci. U. S. A. **107**, 13276 (2010).
[20]N. S. Ginsberg, J. A. Davis, M. Ballottari, Y.-C. Cheng, R. Bassi, and G. R. Fleming, Proc. Natl. Acad. Sci. U. S. A. **108**, 3848 (2011).
[21]D. I. G. Bennett, K. Amarnath, and G. R. Fleming, J. Am. Chem. Soc. **135**, 9164 (2013).
[22]A. Sisto, D. R. Glowacki, and T. J. Martínez, Acc. Chem. Res. **47**, 2857 (2014).
[23]M. D. Fayer, Annu. Rev. Phys. Chem. **60**, 21 (2009).
[24]P. Hamm and M. T. Zanni, *Concepts and Methods of 2D Infrared Spectroscopy* (Cambridge University Press, 2011).
[25]T. A. A. Oliver, N. H. C. Lewis, and G. R. Fleming, Proc. Natl. Acad. Sci. U. S. A. **111**, 10061 (2014), see also corrections on pg. 16628.
[26]M. L. Groot, J. Breton, L. J. G. W. van Wilderen, J. P. Dekker, and R. van Grondelle, J. Phys. Chem. B **108**, 8001 (2004).
[27]A. D. Stahl, M. Di Donato, I. van Stokkum, R. van Grondelle, and M. L. Groot, Biophys. J. **97**, 3215 (2009).
[28]P. Kukura, D. W. McCamant, and R. A. Mathies, Annu. Rev. Phys. Chem. **58**, 461 (2007).
[29]J. A. Cina and P. A. Kovac, J. Phys. Chem. A **117**, 6084 (2013).
[30]H. Dong, N. H. C. Lewis, T. A. A. Oliver, and G. R. Fleming, J. Chem. Phys. **142**, 174201 (2015).
[31]N. H. C. Lewis, H. Dong, T. A. A. Oliver, and G. R. Fleming, J. Chem. Phys. **142**, 174202 (2015).
[32]V. Butkus, L. Valkunas, and D. Abramavicius, J. Chem. Phys. **140**, 034306 (2014).
[33]J. Roden, W. T. Strunz, K. B. Whaley, and A. Eisfeld, J. Chem. Phys. **137**, 204110 (2012).
[34]A. Kolli, E. J. O'Reilly, G. D. Scholes, and A. Olaya-Castro, J. Chem. Phys. **137**, 174109 (2012).
[35]Y. Fujihashi, G. R. Fleming, and A. Ishizaki, J. Chem. Phys. **142**, 212403 (2015).
[36]A. Chenu, N. Christensson, H. F. Kauffmann, and T. Mancal, Sci. Rep. **3**, 2029 (2013).
[37]M. Yang and G. R. Fleming, J. Chem. Phys. **111**, 27 (1999).
[38]M. Yang, K. Ohta, and G. R. Fleming, J. Chem. Phys. **110**, 10243 (1999).
[39]A. G. Redfield, IBM J. Res. Dev. **1**, 19 (1957).
[40]A. G. Redfield, Adv. Magn. Reson. **1**, 1 (1965).
[41]A. Suárez, R. Silbey, and I. Oppenheim, J. Chem. Phys. **97**, 5101 (1992).
[42]A. Ishizaki and G. R. Fleming, J. Chem. Phys. **130**, 234110 (2009).
[43]M. Cho, *Two-Dimensional Optical Spectroscopy* (CRC Press, 2009).
[44]S. Mukamel, *Principles of Nonlinear Optical Spectroscopy* (Oxford University Press, 1995).
[45]F. Duschinsky, Acta Physicochim. URSS **7**, 551 (1937).
[46]G. Herzberg, *Molecular Spectra and Molecular Structure*, Electronic Spectra and Electronic Structure of Polyatomic Molecules (D. Van Nostrand Company, Inc., 1966).
[47]G. J. Small, J. Chem. Phys. **54**, 3300 (2003).
[48]A. Ishizaki and Y. Tanimura, J. Chem. Phys. **125**, 084501 (2006).
[49]A. Ishizaki and Y. Tanimura, J. Phys. Chem. A **111**, 9269 (2007).
[50]M. Di Donato, A. D. Stahl, I. H. M. van Stokkum, R. van Grondelle, and M. L. Groot, Biochemistry **50**, 480 (2011).
[51]Y.-C. Cheng and G. R. Fleming, Annu. Rev. Phys. Chem. **60**, 241 (2009).
[52]A. Ishizaki and G. R. Fleming, Annu. Rev. Condens. Matter Phys. **3**, 333 (2012).
[53]Y. Pang, M. A. Prantil, A. J. Van Tassle, G. A. Jones, and G. R. Fleming, J. Phys. Chem. B **113**, 13086 (2009).
[54]T. A. A. Oliver and G. R. Fleming, J. Phys. Chem. B **119**, 11428 (2015).
[55]I. H. M. van Stokkum, D. S. Larsen, and R. van Grondelle, Biochim. Biophys. Acta, Bioenerg. **1657**, 82 (2004).
[56]L. J. G. W. van Wilderen, C. N. Lincoln, and J. J. van Thor, PLoS One **6**, e17373 (2011).
[57]E. E. Ostroumov, R. M. Mulvaney, R. J. Cogdell, and G. D. Scholes, Science **340**, 52 (2013).
[58]A. Osuka and K. Maruyama, J. Am. Chem. Soc. **110**, 4454 (1988).
[59]N. E. Galanin, L. A. Yakubov, and G. P. Shaposhnikov, Russ. J. Org. Chem. **44**, 921 (2008).
[60]M. C. Chang, P. M. Callahan, P. S. Parkes-Loach, T. M. Cotton, and P. A. Loach, Biochemistry **29**, 421 (2002).
[61]M. A. Harris, P. S. Parkes-Loach, J. W. Springer, J. Jiang, E. C. Martin, P. Qian, J. Jiao, D. M. Niedzwiedzki, C. Kirmaier, J. D. Olsen, D. F. Bocian, D. Holten, C. N. Hunter, J. S. Lindsey, and P. A. Loach, Chem. Sci. **4**, 3924 (2013).
[62]Y. Terazono, G. Kodis, M. Chachisvilis, B. R. Cherry, M. Fournier, A. Moore, T. A. Moore, and D. Gust, J. Am. Chem. Soc. **137**, 245 (2014).
[63]D. Hayes, G. B. Griffin, and G. S. Engel, Science **340**, 1431 (2013).
[64]M. Ferretti, V. I. Novoderezhkin, E. Romero, R. Augulis, A. Pandit, D. Zigmantas, and R. van Grondelle, Phys. Chem. Chem. Phys. **16**, 9930 (2014).
[65]A. Halpin, P. J. M. Johnson, R. Tempelaar, R. S. Murphy, J. Knoester, T. L. C. Jansen, and R. J. D. Miller, Nat. Chem. **6**, 196 (2014).
[66]S. Xie, M. Du, L. Mets, and G. R. Fleming, Proc. SPIE **1640**, 690 (1992).
[67]F. Zhu, C. Galli, and R. M. Hochstrasser, J. Chem. Phys. **98**, 1042 (1993).
[68]A. Matro and J. A. Cina, J. Phys. Chem. **99**, 2568 (1995).
[69]J. M. Dawlaty, D. I. G. Bennett, V. M. Huxter, and G. R. Fleming, J. Chem. Phys. **135**, 044201 (2011).
[70]G. Peter Lepage, J. Comput. Phys. **27**, 192 (1978).